HHS Public Access

Author manuscript

Nucl Med Biol. Author manuscript; available in PMC 2021 May 01.

Published in final edited form as:

Nucl Med Biol. 2020 ; 84-85: 80–87. doi:10.1016/j.nucmedbio.2020.01.004.

Fluorine-18 labeled poly (ADP-ribose) polymerase1 inhibitor as a potential alternative to 2-deoxy-2-[^{18}F]fluoro-D-glucose positron emission tomography in oral cancer imaging.

Paula Demétrio De Souza França[a,b], **Sheryl Roberts**[a], **Susanne Kossatz**[a,1], **Navjot Guru**[a], **Christian Mason**[a], **Daniella Karassawa Zanoni**[b,2], **Marcio Abrahão**[b], **Heiko Schöder**[a], **Ian Ganly**[c,d], **Snehal G. Patel**[c,d,*], **Thomas Reiner**[a,d,e,*]

[a]Department of Radiology, Memorial Sloan Kettering Cancer Center, New York, NY, USA.

[b]Department of Otorhinolaryngology and Head and Neck Surgery, Federal University of São Paulo, SP, Brazil

[c]Department of Surgery, Memorial Sloan Kettering Cancer Center, New York, NY, USA

[d]Weill Cornell Medical College, New York, NY, USA

[e]Chemical Biology Program, Memorial Sloan Kettering Cancer Center, New York, NY, USA

Abstract

Objectives—The evaluation of disease extent and post-therapy surveillance of head and neck cancer using 2-deoxy-2-[^{18}F]fluoro-D-glucose ([^{18}F]FDG) PET is often complicated by physiological uptake in normal tissues of the head and neck region, especially after surgery or radiotherapy. However, irrespective of low positive predictive values, [^{18}F]FDG PET remains the standard of care to stage the disease and monitor recurrences. Here, we report the preclinical use of a targeted poly (ADP-ribose) polymerase1 (PARP1) binding PET tracer, fluorine-18 labeled poly (ADP-ribose) polymerase1 inhibitor ([^{18}F]PARPi), as a potential alternative with greater specificity.

*Correspondence should be addressed to: Thomas Reiner, 1275 York Avenue, New York, NY, 10065, reinert@mskcc.org; (P) 1-646-888-3461; (F) 646 4220408.

Author contributions

P.D.S.F., M.A, S.P. and T.R. conceived the study and designed the experiments. P.D.S.F, S.R., S.K., N.G., C.M. and D.K.Z. carried out the experiments and collected the data. P.D.S.F., C.M., S.P., I.G., H.S., and T.R analyzed the data. S.R. performed synthesis of PARPi-FL, dilution of [^{18}F]FDG and the radiosynthesis of [^{18}F]PARPi. P.D.S.F., N.G. and T.R., wrote IACCUC protocols. P.D.S.F., S.P., I.G. and T.R. conducted statistical analysis of the data. P.D.S.F, S.R., and T.R. primarily wrote the manuscript. All authors carefully read and edited the manuscript.

[1]Additional affiliation: Department of Nuclear Medicine, School of Medicine, Technische Universität München, Munich, Germany

[2]Additional affiliation: Department of Radiology, University of Iowa, IA, USA

Conflict of Interest Statement: S.K., S.P. and T.R. are shareholders of Summit Biomedical Imaging, LLC. S.K., S.P. and T.R. are co-inventors on filed U.S. patent (WO2016164771) that covers methods of use for PARPi-FL. T.R. is co-inventor on U.S. patents (WO2012074840 and WO2016033293), covering the compositions of matter for PARPi-FL and [^{18}F]PARPi, respectively. T.R. is a paid consultant for Theragnostics, Inc.

Data availability

Correspondence and requests for materials should be addressed to T.R.

Methods—Using an orthotopic xenograft mouse model injected with either FaDu or Cal 27 (human squamous cell carcinoma cell lines) we performed PET/CT scans with the 2 tracers and compared the results. Gamma counts and autoradiography were also assessed and correlated with histology.

Results—The average retained activity of [^{18}F]PARPi across cell lines in tumor-bearing tongues was 0.9 ± 0.3 %ID/g, 4.1 times higher than in control (0.2 ± 0.04 %ID/g). Autoradiography and histology confirmed that the activity arose almost exclusively from the tumor areas, with a signal/normal tissue around a ratio of 42.9 ± 21.4. *In vivo*, [^{18}F]PARPi-PET allowed delineation of tumor from healthy tissue ($p < 0.005$), whereas [^{18}F]FDG failed to do so ($p = 0.209$).

Conclusions and implications for patient care—We demonstrate that [^{18}F]PARPi is more specific to tongue tumor tissue than [^{18}F]FDG. [^{18}F]PARPi PET allows for the straightforward delineation of oral cancer in mouse models, suggesting that clinical translation could result in improved imaging of head and neck cancer when compared to [^{18}F]FDG.

Keywords

Fluorine-18 labeled poly (ADP-ribose) polymerase1 inhibitor; [^{18}F]PARPi; 2-deoxy-2-[^{18}F]fluoro-D-glucose; [^{18}F]FDG; PET/CT; oral cancer; squamous cell carcinoma

INTRODUCTION

2-deoxy-2-[^{18}F]fluoro-D-glucose ([^{18}F]FDG) positron emission tomography (PET) is a valuable tool for the diagnosis and post-treatment surveillance of patients in head and neck oncology [1]. The tracer is used to determine the pretreatment extent of disease, to help identify unknown primary tumors and second synchronous primary tumors, to access response to therapy, and to monitor the patient for post-treatment recurrence and/or persistence [2–4]. However, although [^{18}F]FDG is a valuable and powerful standard-of-care PET tracer for oncologic head and neck imaging [5–8], it does have certain disadvantages that can perturb image interpretation. [^{18}F]FDG is a glucose-mimicking metabolic tracer, which can be retained not only in malignant tumors, but also in several normal tissues with glucose avidity [1]. This can be particularly problematic in the head and neck region, which is inherently metabolically active and structurally complex [3, 9].

While physiologic uptake in benign tissue does complicate [^{18}F]FDG interpretation, the uptake in healthy benign structures is typically symmetrical, improving the accuracy of initial diagnosis of cancer [1, 3]. However, in cases of suspected recurrence, when a patient has already undergone surgery and/or radiation therapy, the pattern of [^{18}F]FDG uptake and the anatomical landmarks seen on computed tomography (CT) will often be asymmetrical, making interpretation much more difficult [1, 10]. Other benign conditions, such as nerve palsy and inflammation, could also lead to erroneous readouts due to metabolic imbalance in normal structures [10, 11]. Additionally, very small primary tumors could escape detection if located close to or within areas of high physiological uptake. Intuitively, these limitations reduce the value of [^{18}F]FDG PET as an oncologic imaging modality for head and neck cancer in general and particularly for oral cancers. While the sensitivity ranges from 87% to 97% and specificity from 76% to 86% for making diagnoses [6], positive predictive values

(PPVs) as low as 68–82% are reported for the identification of locoregional persistence or recurrence with [^{18}F]FDG [6, 12, 13].

In an attempt to address this unmet clinical need, we investigated fluorine-18 labeled poly (ADP-ribose) polymerase1 inhibitor ([^{18}F]PARPi) [14] as an alternative. Tumor detection with this tracer is not based on metabolic activity but relies rather on the presence of the DNA-repair enzyme poly (ADP-ribose) polymerase1 (PARP1) in tumor nuclei. Studies have shown that both oral and oropharyngeal cancer overexpress PARP1 at high levels relative to normal and dysplastic tissues [15–17].

The molecular structure of [^{18}F]PARPi is based on the phthalazin-1(*2H*)-one scaffold of Olaparib, a PARP1 inhibitor used as a therapeutic agent in gynecological malignancies [14]. Other PARP1-targeted tracers have been developed as well and used both in the preclinical [18–27] and clinical [28–30] setting. Several reviews have categorized different approaches to image PARP1 *in vivo* [31, 32]. After injection, [^{18}F]PARPi accumulates preferentially in the nuclei of tumor cells and not in metabolically active muscle tissue. This supports our central hypothesis that [^{18}F]PARPi is capable of imaging head and neck tumors with higher contrast than [^{18}F]FDG.

MATERIALS AND METHODS

All information regarding general methods, chemicals, cell lines, cell culture, PARPi-FL stain, confocal imaging, and western blot can be found in the supplementary files. Fig. 1 shows the study schema.

Statistical analysis

Statistical analysis was performed using GraphPad Prism 7. Data points represent mean values, and error bars represent standard deviations. We used the Mann-Whitney test for analysis of unpaired samples (e.g. [^{18}F]PARPi uptake in xenografted tongues and in control tongues from different mice) and Wilcoxon test for analysis of paired samples (e.g. PARP1-positive area of tongue tumor, skeletal muscle, salivary gland, fat and brain tissue on the same mouse). Statistical significance was determined with alpha = 0.05 and the level of significance for each result displayed as *$p < 0.05$, **$p < 0.01$, ***$p < 0.001$, and ****$p < 0.0001$. All experiments subjected to statistical analysis consisted of group sizes of at least 3.

PARPi-FL synthesis, [^{18}F]FDG preparation and [^{18}F]PARPi radiosynthesis

PARPi-FL was synthesized according to our previously described procedure [33–35]; a detailed description can also be found in the supplementary methods. [^{18}F]FDG was obtained from the Radiochemistry and Molecular Imaging Probes Core, Memorial Sloan Kettering Cancer Center (MSK). [^{18}F]PARPi was synthesized using an optimized labeling procedure according to our previously described method [14, 35, 36], described in the supplementary methods. Reaction and purity of the compounds can be found in Supplementary Fig. 1 (PARPi-FL) and Supplementary Fig. 2 ([^{18}F]PARPi).

Animals and xenografting

All animal experiments were performed in accordance with protocols approved by the Institutional Animal Care and Use Committee of MSK and followed the National Institute of Health guidelines for animal welfare. Nineteen athymic nude mice 6–8 weeks old were purchased from Envigo RMS, Inc. Seven of them were inoculated on the anterior 1/3 and ventral portion of the right-hand side of the tongue with 500,000 cancer cells in 20 μL of PBS (n = 3 FaDu, n = 4 Cal 27), and tumors were allowed to proliferate for 4 weeks to a tumor size ranging from 0.4 to 0.7 cm. The other 12 healthy mice were used as controls.

PET/CT imaging

Mice were injected with an average of 7.7 ± 2.2 MBq (208.1 ± 59.4 μCi) of [^{18}F]FDG on Day 1 after tumor establishment and an average of 10.4 ± 3 MBq (282.2 ± 80.6 μCi) of [^{18}F]PARPi on Day 2. Animals underwent fasting for 8 hours prior to [^{18}F]FDG imaging. No fasting was required for [^{18}F]PARPi imaging. Animals were imaged on an INVEON small-animal micro-PET/CT scanner (Siemens, Knoxville, TN, United States) under isoflurane-induced (Baxter Healthcare, Piramal Enterprises Limited, India) anesthesia. A whole-body static PET scan was performed, and data was recorded for 10 minutes, with 50 million coincidence events, 90 minutes post-injection. Imaging data was normalized to correct for nonuniform PET response, dead-time count losses, positron branching ratio, and physical decay to the time of injection. The counting rates in the reconstructed images were converted to activity concentrations (%ID/g) using a system calibration factor derived from imaging a mouse-sized water-equivalent phantom containing [^{18}F]. Images were analyzed using Inveon Research Workspace (Siemens Healthiness Global) software, with the CT component of the experiment used for anatomical reference. Activity concentrations were quantified by averaging the mean values of five regions of interest drawn on consecutives slices of tongues, submandibular salivary gland, brown fat, skeletal muscle (taken from the right thigh) and brain. In the volume of interest quantification 1 mL is assumed to be 1 gram.

Autoradiography and γ-counting

Animals were intravenously injected with an average of 10.4 ± 3 MBq (282.2 ± 80.6 μCi) of [^{18}F]PARPi. After PET imaging was completed, the animals were euthanized; tongues were harvested, weighed, and counted in a Wizard^2 automatic γ-counter (PerkinElmer, Boston, MA). The radiopharmaceutical uptake was expressed as a percentage of injected dose per gram (%ID/g) using the following formula: [(activity in the tongue/grams of tissue)/injected dose] × 100%. Immediately afterwards, gamma counting specimens were flash frozen in Optimal Cutting Temperature Embedding Medium using dry ice. Slides were prepared with 10 μm cryosections of the tissue using a cryotome. One section from each tumor-bearing tongue and one section from each control tongue (n = 7 tumors; 3 FaDu, 4 Cal 27, and 12 control tongues) were exposed to an autoradiography plate for 12 hours and read with a Typhoon FLA 7000 laser scanner from GE Healthcare (Port Washington, NY). Fiji (ImageJ) was used to quantify the intensity of signal of each part of the tissue. Five areas of interest (ROIs) were taken from tumor and normal adjacent muscle for the xenografted mice and 5 ROIs from the control tongues. Results were obtained using the average of those ROIs, expressing a tumor-to-normal-tongue ratio. The same slides exposed to the autoradiography

plate were subsequently stained with hematoxylin and eosin stain (H&E) for histological confirmation of tumor presence. Slides were scanned (Mirax, 3DHISTECH, Budapest, Hungary) to allow for digital histological correlation with autoradiography data (see supplementary methods for details).

RESULTS

Oral cancer cell lines express PARP1 and show uptake of PARP imaging agents

Western blot analysis confirmed that both Cal 27 and FaDu cells were expressing PARP1, corroborating data from previous reports [15, 16, 25]. Our results show that both cell lines expressed PARP1 to a significant degree, allowing further experiments to proceed (Fig. 2A). We next showed specific uptake of PARP inhibitors in cells by using PARPi-FL, a fluorescently tagged version of the pthalazin-1(*2H*)-one Olaparib. Briefly, the cyclopropane group of Olaparib was replaced by the green fluorescent BODIPY-FL [33, 34]. (Supplementary Fig. 1.) PARPi-FL showed to be highly specific for PARP1. Our microscopy images of tumor cells showed abundant specific nuclear PARPi-FL in the nuclei of both cell lines. Specificity was confirmed using the nuclear stain Hoechst (Fig. 2B).

[^{18}F]PARPi tracer uptake in tumor-bearing tongues was significantly higher than in healthy controls

To demonstrate tumor uptake of [^{18}F]PARPi, we measured gamma activity in the xenografted tongues and in the control tongues. The average tracer uptake in the xenografted tongues (n = 7) after [^{18}F]PARPi injection was 0.9 ± 0.3 %ID/g. When breaking down the uptake by the two different cell lines, tongues xenografted with FaDu (n = 3) had a slightly higher average of 0.9 ± 0.4 %ID/g, compared to Cal 27 (n = 4), which had an average of 0.8 ± 0.3 %ID/g. Although the FaDu cells retained a slightly higher amount of [^{18}F]PARPi, we did not observe any statistical significance between the 2 cohorts ($p = 0.86$). Compared to the xenograft mice, healthy tongues (n = 12), retained a much lower amount of activity (0.2 ± 0.04 %ID/g, $p < 0.0001$ for both FaDu and Cal 27, Fig. 3A).

[^{18}F]PARPi autoradiography demonstrated that tracer retention is almost exclusively confined to orthotopic tumor

Autoradiography of frozen section slides, taken from the xenografted and the control tongues, were performed and results were correlated with histology to determine activity source. By doing so, it was possible to demonstrate that the overwhelming majority of activity in xenografted tongues arose from orthotopic tumors. In addition, a low amount of uptake was also detected in control tongues. (Fig. 3B) Histology suggests that it arose from the basal layer of the squamous epithelium of the tongue. This result was compared to earlier work [15, 16], where PARP expression was found in cells — the originating tissue compartment of squamous cell carcinoma. In contrast, control tongues had almost no uptake (Fig. 3C). We were able to delineate the tumor areas using autoradiography, yielding a tumor-to-normal-tissue ratio of 42.9 ± 21.4. Analyzing the cell lines separately, FaDu yielded a tumor-to-normal tissue ratio of 39.1 ± 24.7 and Cal 27 45.8 ± 2, with no statistical significance between them ($p > 0.99$) (Fig. 3B).

[^{18}F]PARPi PET/CT showed improved tumor delineation relative to [^{18}F]FDG in mouse tongue xenografts

In order to verify that [^{18}F]PARPi allows for more specific tumor delineation than standard-of-care [^{18}F]FDG, individual mice were scanned with one tracer one day and another the next, and results were compared. [^{18}F]FDG scans from tumor-bearing and healthy mice presented with high physiological uptake in tongue, floor of mouth, and masticatory muscles, even though mice underwent fasting for 8 hours and were maintained under isoflurane anesthesia during imaging. The mean uptake in the tumor-bearing tongues was 6.5 ± 2 %ID/g, whereas in controls it was 7.6 ± 3.4 %ID/g ($p = 0.84$, Supplementary Fig. 3). With [^{18}F]FDG, it was not possible to differentiate tumor-bearing from healthy tongues or delineate tumor from surrounding normal tissue within tumor-bearing tongues. (Fig. 4A). High [^{18}F]FDG uptake in tumor-bearing mice was also seen in the salivary glands (3.9 ± 1.6 %ID/g), skeletal muscle (8.6 ± 3.4 %ID/g) and brain (7.2 ± 4.6 %ID/g) with no statistical significance when compared to the xenografted tongue ($p = 0.08$; $p = 0.30$; and $p = 0.58$, respectively). Moderate uptake was seen in brown fat (1.3 ± 0.4 %ID/g). Fat was the only tissue that had a significantly lower uptake in healthy mice relative to tumor-bearing mice ($p < 0.05$, Fig. 4B).

In contrast, [^{18}F]PARPi showed clear uptake in all xenografted tongue tumors, while uptake in the surrounding normal tongue was low, allowing it to differentiate tumor from surrounding normal tongue (Fig. 4A and Supplementary Fig. 4). The mean [^{18}F]PARPi uptake in the tumor was 1.2 ± 0.4 %ID/g, whereas in the tongues of control mice we found uptake levels of 0.2 ± 0.1 %ID/g ($p < 0.001$ [Fig. 4B, Supplementary Fig. 4]). Compared to tumor uptake, [^{18}F]PARPi accumulation within the tumor-bearing mice was lower in the salivary glands (0.8 ± 0.3 %ID/g, $p < 0.05$), fat tissue (0.3 ± 0.2 %ID/g, $p<0.05$), skeletal muscle (0.3 ± 0.3 %ID/g, $p < 0.05$) and brain (0.2 ± 0.1 %ID/g, $p < 0.005$) (Fig. 4B). [^{18}F]FDG uptake in the xenografted tongues was not significantly different ($p > 0.05$) from the controls, whereas in [^{18}F]PARPi it was ($p < 0.001$), demonstrating the new tracer's great potential for head and neck imaging (Fig. 5).

DISCUSSION

In this study, we investigated the feasibility of using the PARP1 imaging agent [^{18}F]PARPi to delineate orthotopic oral squamous cell carcinomas in mouse models. We found that [^{18}F]PARPi specifically accumulated in tumor areas but not healthy tongue, leading to high tumor-to-normal-tissue ratios. In contrast, the standard-of-care imaging agent [^{18}F]FDG showed high uptake in tumors, surrounding normal tongue and healthy tongues, compounding tumor delineation.

[^{18}F]PARPi is based on the scaffold of Olaparib, a PARP inhibitor used most commonly for the treatment of breast and ovarian cancer [37]. By replacing the cyclopropane group of this small molecule [14], we are able to maintain its specificity. Although chemically different, both PARPi-FL and [^{18}F]PARPi are selective inhibitors of PARP1, since both modifications are made on a region of the Olaparib scaffold that is not essential for target binding. Both compounds have near-identical inhibition profiles [33, 38–40].

PARP1 is one of the most abundantly expressed nuclear enzymes and plays a key role in cell signaling, DNA damage response, and a variety of other biological pathways [41]. It is known that this enzyme is expressed not only in tumors but also in normal tissue, such as the epithelial basal layer [15]. However, during tumor development, PARP1 is generally upregulated relative to normal tissues [15]. This PARP1 overexpression is what generates tumor contrast in a PET/CT scan after injection of [^{18}F]PARPi [23, 27]. Although different malignancies usually present unique characteristics when defined by tissue of origin and genetic mutations, the underlying biochemical function of the PARP enzyme remains universal [23], which gives [^{18}F]PARPi the potential for use in a wide range of tumors [15, 24, 28, 30–32, 42]. The synthesis of [^{18}F]PARPi and its cold analogue [^{19}F]PARPi has been published using a glioblastoma mouse model [14]. The IC_{50}, biodistribution, blood half-life and stability have also been previously reported [14].

We also demonstrated specific, nuclear *in vitro* uptake using PARPi-FL (the fluorescent version of the PARP inhibitor), analogous to previous reports [16, 25]. Autoradiography of tumor-bearing mice and healthy controls showed that the tracer was retained at much higher levels in the diseased mouse tongues. Using H&E as the gold standard, and overlaying the H&E images with those obtained with autoradiography, we confirmed co-localization of [^{18}F]PARPi uptake and tumor cells. Almost no radioactivity was detected in the normal muscle or in the control tongues, corroborating our hypothesis that tumor delineation is possible based of the differential expression of PARP1.

Our results demonstrated that, in mouse tongue xenografts, [^{18}F]PARPi can detect head and neck tumors using PET/CT. Most significantly, our data suggests improved tumor delineation relative to [^{18}F]FDG, the current gold standard PET tracer used in head and neck oncology. In humans, [^{18}F]FDG has a good sensitivity, ranging from 87% to 97%; specificity ranges from 76% to 86% [6, 13]. Due to its high physiological uptake in normal structures, its PPVs for cancer diagnoses in head and neck oncology [4] are low, reported to range from 68 to 82% [6, 12]. We have demonstrated that [^{18}F]PARPi, a tracer not based on metabolic activity, was able to overcome this problem in mice, showing improved tumor delineation on xenografted tongues.

Another important consideration is that, while patients are asked to rest before injection of [^{18}F]FDG in order to reduce unspecific muscular uptake, [^{18}F]PARPi imaging can be conducted without the need for resting or fasting. For oral cancer patients, especially those with large bulky tumors in the mouth and those who have had local anatomy and physiology altered because of treatment, resting can become very difficult. Patients require tongue movement to be able to maintain normal physiological activities such as breathing, talking or swallowing saliva. The tongue's muscular activity can be particularly high in cases of previous partial glossectomy or unilateral hypoglossal palsy because of physiological compensation on the moving side.

Typically, mouse experiments using [^{18}F]FDG are performed on mice that have been anesthetized from the point of injection to the completion of imaging to minimize muscle uptake [43, 44]. Here, however, we believe that this practice would not have accurately reflected our clinical question. Therefore, mice were kept awake after injection and

underwent anesthesia only during imaging. Aside from this, all scans were conducted in the morning after fasting overnight.

This study has some limitations. Being nocturnal, mice are more active at night, which might explain the higher uptake of [^{18}F]FDG in skeletal muscle seen in this study [43, 44]. It is important to emphasize that [^{18}F]PARPi, different from [^{18}F]FDG, is not a metabolic tracer, and therefore it appears unlikely that rest or fasting is necessary prior to the scans. Besides this, our xenografted mice had large tongue tumors when compared to their body mass, which is not always the case for patients. Because our preclinical PET/CT has a limited resolution (4.2 mm^3, corresponding to a spherical lesion of 2 mm diameter) it may not detect very small lesions. Therefore, we allowed tumors to grow to at least 4 mm in diameter before imaging.

[^{18}F]FDG PET/CT is a valuable tool for head and neck oncologic imaging and works well is most scenarios. Several studies have reported its use for the detection of tumors, staging and post-treatment surveillance of patients [6, 13]. A prospective, randomized controlled trial published in 2016 revealed similar survival among patients in the 2 study groups: the ones who underwent surveillance with scheduled [^{18}F]FDG PET/CT and the group who underwent surgery (planned neck dissections) [45], illustrating the tracer's important role in head and neck imaging. In the future, translational efforts will be necessary to evaluate the potential value of [^{18}F]PARPi in addition to the existing standard-of-care practices.

CONCLUSION

We have demonstrated the ability of [^{18}F]PARPi PET/CT to image oral cancer and improve tumor delineation when compared to [^{18}F]FDG. [^{18}F]PARPi could be of great clinical interest, as it appears to provide higher contrast ratios than [^{18}F]FDG in tongue tissues. This technology could be particularly important for patients with oral cancer, in which physiological uptake of [^{18}F]FDG is usually high due to involuntary and/or compensatory tongue movements.

Supplementary Material

Refer to Web version on PubMed Central for supplementary material.

Acknowledgments

The authors gratefully acknowledge the support of the Memorial Sloan Kettering Cancer Animal Imaging Core, Radiochemistry & Molecular Imaging Probes Core, Molecular Cytology Core and the Nuclear Magnetic Resonance Analytical Core facilities. We also thank Scott Garon and Jessica Massler for editing the manuscript, and Dr. Kishore Pillarsetty for helpful discussions.

Financial Support

This work was supported by National Institutes of Health grants P30 CA008748, R01 CA204441 (TR), R43 CA228815 (CB), and K99 CA218875 (SK). The authors thank the MSK Center for Molecular Imaging & Nanotechnology, the MSK Imaging and Radiation Sciences Program, and the MSK Molecularly Targeted Intraoperative Imaging Fund. The funding sources were not involved in study design, data collection and analysis, writing of the report, or the decision to submit this article for publication.

Abbreviations:

PARP1	poly (ADP ribose) polymerase1
[^{18}F]FDG	2-deoxy-2-[^{18}F]fluoro-D-glucose
PET	positron emission tomography
CT	computed tomography
PPV	positive predictive value
MSK	Memorial Sloan Kettering Cancer Center
ROI	area of interest
H & E	Hematoxylin and eosin stain

References

[1]. Meerwein CM, Queiroz M, Kollias S, Hullner M, Veit-Haibach P, and Huber GF. Posttreatment surveillance of head and neck cancer: pitfalls in the interpretation of FDG PET-CT/MRI. Swiss medical weekly 2015;145:w14116. [PubMed: 25701645]

[2]. Manca G, Vanzi E, Rubello D, Giammarile F, Grassetto G, Wong KK, et al. (18)F-FDG PET/CT quantification in head and neck squamous cell cancer: principles, technical issues and clinical applications. European journal of nuclear medicine and molecular imaging 2016;43:1360–75. [PubMed: 26780912]

[3]. Al-Ibraheem A, Buck A, Krause BJ, Scheidhauer K, and Schwaiger M. Clinical Applications of FDG PET and PET/CT in Head and Neck Cancer. Journal of oncology 2009;2009:208725. [PubMed: 19707528]

[4]. Ng SH, Yen TC, Liao CT, Chang JT, Chan SC, Ko SF, et al. 18F-FDG PET and CT/MRI in oral cavity squamous cell carcinoma: a prospective study of 124 patients with histologic correlation. Journal of nuclear medicine : official publication, Society of Nuclear Medicine 2005;46:1136–43.

[5]. Galgano SJ, Marshall RV, Middlebrooks EH, McConathy JE, and Bhambhvani P. PET/MR Imaging in Head and Neck Cancer: Current Applications and Future Directions. Magn Reson Imaging Clin N Am 2018;26:167–78. [PubMed: 29128003]

[6]. Isles MG, McConkey C, and Mehanna HM. A systematic review and meta-analysis of the role of positron emission tomography in the follow up of head and neck squamous cell carcinoma following radiotherapy or chemoradiotherapy. Clinical otolaryngology : official journal of ENT-UK ; official journal of Netherlands Society for Oto-Rhino-Laryngology & Cervico-Facial Surgery 2008;33:210–22.

[7]. Schoder H, Fury M, Lee N, and Kraus D. PET monitoring of therapy response in head and neck squamous cell carcinoma. Journal of nuclear medicine : official publication, Society of Nuclear Medicine 2009;50 Suppl 1:74s–88s.

[8]. Lim R, Eaton A, Lee NY, Setton J, Ohri N, Rao S, et al. 18F-FDG PET/CT metabolic tumor volume and total lesion glycolysis predict outcome in oropharyngeal squamous cell carcinoma. Journal of nuclear medicine : official publication, Society of Nuclear Medicine 2012;53:1506–13.

[9]. Hojgaard L, Berthelsen AK, and Loft A. Head and neck: normal variations and benign findings in FDG positron emission tomography/computed tomography imaging. PET clinics 2014;9:141–5. [PubMed: 25030278]

[10]. Chow Z, McIvor J, McDonnell O, and Khaleel Z. False-positive uptake of 18F-FDG in hypoglossal nerve palsy following chemoradiotherapy for tongue base cancer. ANZ journal of surgery 2016;86:313–4. [PubMed: 24845760]

[11]. Metser U, Miller E, Lerman H, and Even-Sapir E. Benign nonphysiologic lesions with increased 18F-FDG uptake on PET/CT: characterization and incidence. AJR. American journal of roentgenology 2007;189:1203–10. [PubMed: 17954662]

[12]. Abgral R, Querellou S, Potard G, Le Roux PY, Le Duc-Pennec A, Marianovski R, et al. Does 18F-FDG PET/CT improve the detection of posttreatment recurrence of head and neck squamous cell carcinoma in patients negative for disease on clinical follow-up? Journal of nuclear medicine : official publication, Society of Nuclear Medicine 2009;50:24–9.

[13]. Gupta T, Master Z, Kannan S, Agarwal JP, Ghsoh-Laskar S, Rangarajan V, et al. Diagnostic performance of post-treatment FDG PET or FDG PET/CT imaging in head and neck cancer: a systematic review and meta-analysis. European journal of nuclear medicine and molecular imaging 2011;38:2083–95. [PubMed: 21853309]

[14]. Carney B, Carlucci G, Salinas B, Di Gialleonardo V, Kossatz S, Vansteene A, et al. Non-invasive PET Imaging of PARP1 Expression in Glioblastoma Models. Molecular imaging and biology : MIB : the official publication of the Academy of Molecular Imaging 2016;18:386–92. [PubMed: 26493053]

[15]. Kossatz S, Pirovano G, De Souza França PD, Strome AL, Sunny SP, Zanoni DK, et al. PARP1 as a biomarker for early detection and intraoperative tumor delineation in epithelial cancers – first-in-human results. bioRxiv 2019:663385.

[16]. Kossatz S, Brand C, Gutiontov S, Liu JT, Lee NY, Gonen M, et al. Detection and delineation of oral cancer with a PARP1 targeted optical imaging agent. Scientific reports 2016;6:21371. [PubMed: 26900125]

[17]. Tang J, Salloum D, Carney B, Brand C, Kossatz S, Sadique A, et al. Targeted PET imaging strategy to differentiate malignant from inflamed lymph nodes in diffuse large B-cell lymphoma. Proceedings of the National Academy of Sciences of the United States of America 2017;114:E7441–e9. [PubMed: 28827325]

[18]. Pirovano G, Jannetti SA, Carter LM, Sadique A, Kossatz S, Guru N, et al. Targeted brain tumor radiotherapy using an Auger emitter. bioRxiv 2019:649764.

[19]. Jannetti SA, Carlucci G, Carney B, Kossatz S, Shenker L, Carter LM, et al. PARP-1-Targeted Radiotherapy in Mouse Models of Glioblastoma. Journal of nuclear medicine : official publication, Society of Nuclear Medicine 2018;59:1225–33.

[20]. Gonzales J, Kossatz S, Roberts S, Pirovano G, Brand C, Perez-Medina C, et al. Nanoemulsion-Based Delivery of Fluorescent PARP Inhibitors in Mouse Models of Small Cell Lung Cancer. Bioconjugate chemistry 2018;29:3776–82. [PubMed: 30354077]

[21]. Wilson TC, Xavier MA, Knight J, Verhoog S, Torres JB, Mosley M, et al. PET Imaging of PARP Expression Using (18)F-Olaparib. Journal of nuclear medicine : official publication, Society of Nuclear Medicine 2019;60:504–10.

[22]. Zhou D, Xu J, Mpoy C, Chu W, Kim SH, Li H, et al. Preliminary evaluation of a novel (18)F-labeled PARP-1 ligand for PET imaging of PARP-1 expression in prostate cancer. Nuclear medicine and biology 2018;66:26–31. [PubMed: 30195072]

[23]. Sander Effron S, Makvandi M, Lin L, Xu K, Li S, Lee H, et al. PARP-1 Expression Quantified by [(18)F]FluorThanatrace: A Biomarker of Response to PARP Inhibition Adjuvant to Radiation Therapy. Cancer Biother Radiopharm 2017;32:9–15. [PubMed: 28118040]

[24]. Makvandi M, Xu K, Lieberman BP, Anderson RC, Effron SS, Winters HD, et al. A Radiotracer Strategy to Quantify PARP-1 Expression In Vivo Provides a Biomarker That Can Enable Patient Selection for PARP Inhibitor Therapy. Cancer research 2016;76:4516–24. [PubMed: 27261505]

[25]. Kossatz S, Weber WA, and Reiner T. Optical Imaging of PARP1 in Response to Radiation in Oral Squamous Cell Carcinoma. PloS one 2016;11:e0147752. [PubMed: 26808835]

[26]. Salinas B, Irwin CP, Kossatz S, Bolaender A, Chiosis G, Pillarsetty N, et al. Radioiodinated PARP1 tracers for glioblastoma imaging. EJNMMI research 2015;5:123. [PubMed: 26337803]

[27]. Edmonds CE, Makvandi M, Lieberman BP, Xu K, Zeng C, Li S, et al. [(18)F]FluorThanatrace uptake as a marker of PARP1 expression and activity in breast cancer. American journal of nuclear medicine and molecular imaging 2016;6:94–101. [PubMed: 27069769]

[28]. Michel LS, Dyroff S, Brooks FJ, Spayd KJ, Lim S, Engle JT, et al. PET of Poly (ADP-Ribose) Polymerase Activity in Cancer: Preclinical Assessment and First In-Human Studies. Radiology 2017;282:453–63. [PubMed: 27841728]

[29]. Michel LS, Dyroff S, Brooks FJ, Spayd KJ, Lim S, Engle JT, et al. PET of Poly (ADP-Ribose) Polymerase Activity in Cancer: Preclinical Assessment and First In-Human Studies. Radiology 2019;291:271. [PubMed: 30897045]

[30]. Makvandi M, Pantel A, Schwartz L, Schubert E, Xu K, Hsieh CJ, et al. A PET imaging agent for evaluating PARP-1 expression in ovarian cancer. The Journal of clinical investigation 2018;128:2116–26. [PubMed: 29509546]

[31]. Knight JC, Koustoulidou S, and Cornelissen B. Imaging the DNA damage response with PET and SPECT. European journal of nuclear medicine and molecular imaging 2017;44:1065–78. [PubMed: 28058462]

[32]. Carney B, Kossatz S, and Reiner T. Molecular Imaging of PARP. Journal of nuclear medicine : official publication, Society of Nuclear Medicine 2017;58:1025–30.

[33]. Reiner T, Lacy J, Keliher EJ, Yang KS, Ullal A, Kohler RH, et al. Imaging therapeutic PARP inhibition in vivo through bioorthogonally developed companion imaging agents. Neoplasia (New York, N.Y.) 2012;14:169–77.

[34]. Irwin CP, Portorreal Y, Brand C, Zhang Y, Desai P, Salinas B, et al. PARPi-FL--a fluorescent PARP1 inhibitor for glioblastoma imaging. Neoplasia (New York, N.Y.) 2014;16:432–40.

[35]. Carney B, Kossatz S, Lok BH, Schneeberger V, Gangangari KK, Pillarsetty NVK, et al. Target engagement imaging of PARP inhibitors in small-cell lung cancer. Nature communications 2018;9:176.

[36]. Kossatz S, Carney B, Schweitzer M, Carlucci G, Miloushev VZ, Maachani UB, et al. Biomarker-Based PET Imaging of Diffuse Intrinsic Pontine Glioma in Mouse Models. Cancer research 2017;77:2112–23. [PubMed: 28108511]

[37]. Scott CL, Swisher EM, and Kaufmann SH. Poly (ADP-ribose) polymerase inhibitors: recent advances and future development. J Clin Oncol 2015;33:1397–406. [PubMed: 25779564]

[38]. Carlucci G, Carney B, Brand C, Kossatz S, Irwin CP, Carlin SD, et al. Dual-Modality Optical/PET Imaging of PARP1 in Glioblastoma. Molecular imaging and biology : MIB : the official publication of the Academy of Molecular Imaging 2015;17:848–55. [PubMed: 25895168]

[39]. Reiner T, Keliher EJ, Earley S, Marinelli B, and Weissleder R. Synthesis and in vivo imaging of a 18F-labeled PARP1 inhibitor using a chemically orthogonal scavenger-assisted high-performance method. Angewandte Chemie (International ed. in English) 2011;50:1922–5. [PubMed: 21328671]

[40]. Reiner T, Earley S, Turetsky A, and Weissleder R. Bioorthogonal small-molecule ligands for PARP1 imaging in living cells. Chembiochem : a European journal of chemical biology 2010;11:2374–7. [PubMed: 20967817]

[41]. Jubin T, Kadam A, Jariwala M, Bhatt S, Sutariya S, Gani AR, et al. The PARP family: insights into functional aspects of poly (ADP-ribose) polymerase-1 in cell growth and survival. Cell proliferation 2016;49:421–37. [PubMed: 27329285]

[42]. Morales J, Li L, Fattah FJ, Dong Y, Bey EA, Patel M, et al. Review of poly (ADP-ribose) polymerase (PARP) mechanisms of action and rationale for targeting in cancer and other diseases. Crit Rev Eukaryot Gene Expr 2014;24:15–28. [PubMed: 24579667]

[43]. Lee KH, Ko BH, Paik JY, Jung KH, Choe YS, Choi Y, et al. Effects of anesthetic agents and fasting duration on 18F-FDG biodistribution and insulin levels in tumor-bearing mice. Journal of nuclear medicine : official publication, Society of Nuclear Medicine 2005;46:1531–6.

[44]. Fueger BJ, Czernin J, Hildebrandt I, Tran C, Halpern BS, Stout D, et al. Impact of animal handling on the results of 18F-FDG PET studies in mice. Journal of nuclear medicine : official publication, Society of Nuclear Medicine 2006;47:999–1006.

[45]. Mehanna H, Wong WL, McConkey CC, Rahman JK, Robinson M, Hartley AG, et al. PET-CT Surveillance versus Neck Dissection in Advanced Head and Neck Cancer. The New England journal of medicine 2016;374:1444–54. [PubMed: 27007578]

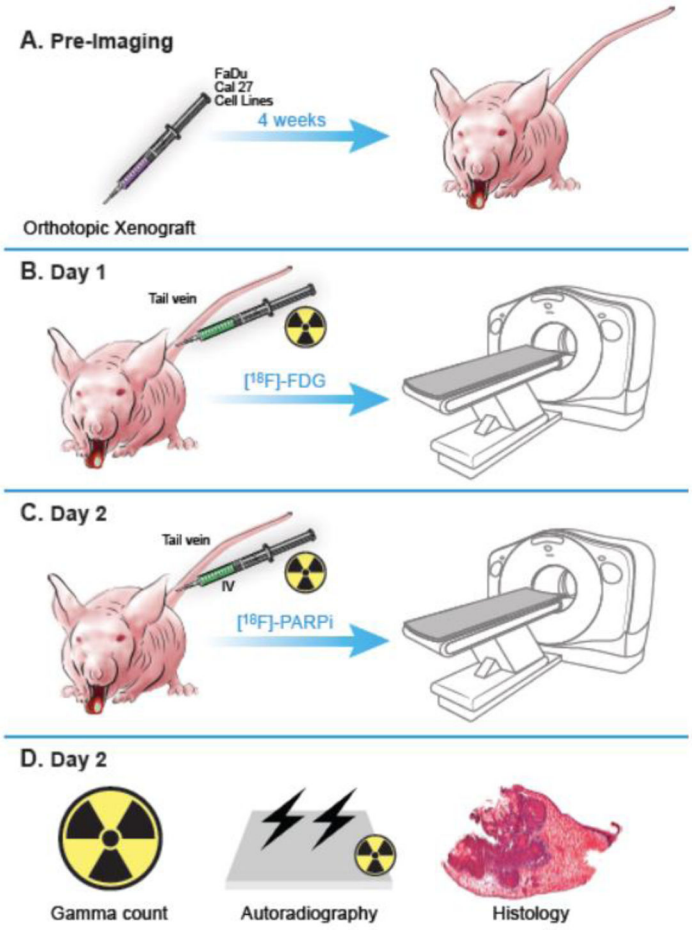

Fig 1.

Scheme of the study design and workflow. All animal experiments were performed in accordance with protocols approved by the Institutional Animal Care and Use Committee (IACUC) of MSK and followed the National Institute of Health guidelines for animal welfare. **(A)** Animals were inoculated on the anterior 1/3 and ventral portion of the right-hand side of the tongue with 500,000 cancer cells in 20 μL of PBS (n = 3 FaDu, n = 4 Cal 27), and tumors were allowed to proliferate for 4 weeks. **(B)** Mice were intravenously (tail vein) injected with an average of 7.7 ± 2.2 MBq (208.1 ± 59.4 μCi) of [^{18}F]FDG on Day 1 after tumor establishment, and imaged 90 minutes after injection, under isoflurane anesthesia for 15 minutes. **(C)** The same animals were injected with an average of 10.4 ± 3 MBq (282.2 ± 80.6 μCi) of [^{18}F]PARPi on Day 2, and imaged 90 minutes after injection. All animals were imaged on an INVEON small-animal micro-PET/CT scanner under isoflurane-induced anesthesia. **(D)** After [^{18}F]PARPi imaging, animals were euthanized, and their tongues were harvested for radiation gamma-counting, autoradiography, and H&E staining.

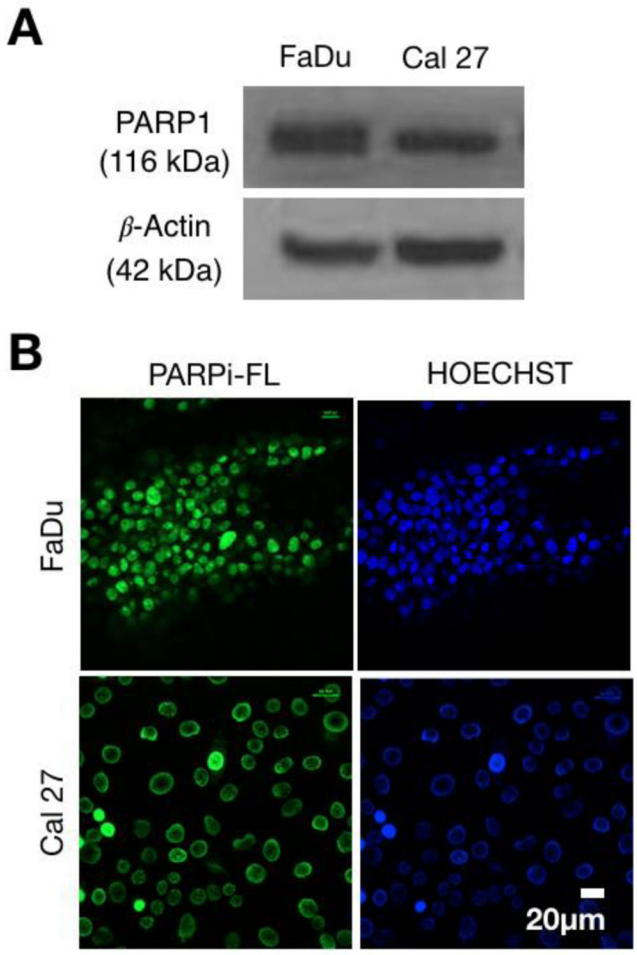

Fig 2.

PARP1 expression in FaDu and Cal 27 and PARPi-FL *in vitro* uptake. **(A)** Western Blot analysis of FaDu and Cal 27 cells, showing expression of PARP1 in both cell lines. **(B)** *In vitro* uptake of PARPi-FL, together with nuclear Hoechst 33342 uptake in FaDu (top row) Cal 27 (bottom row) cells.

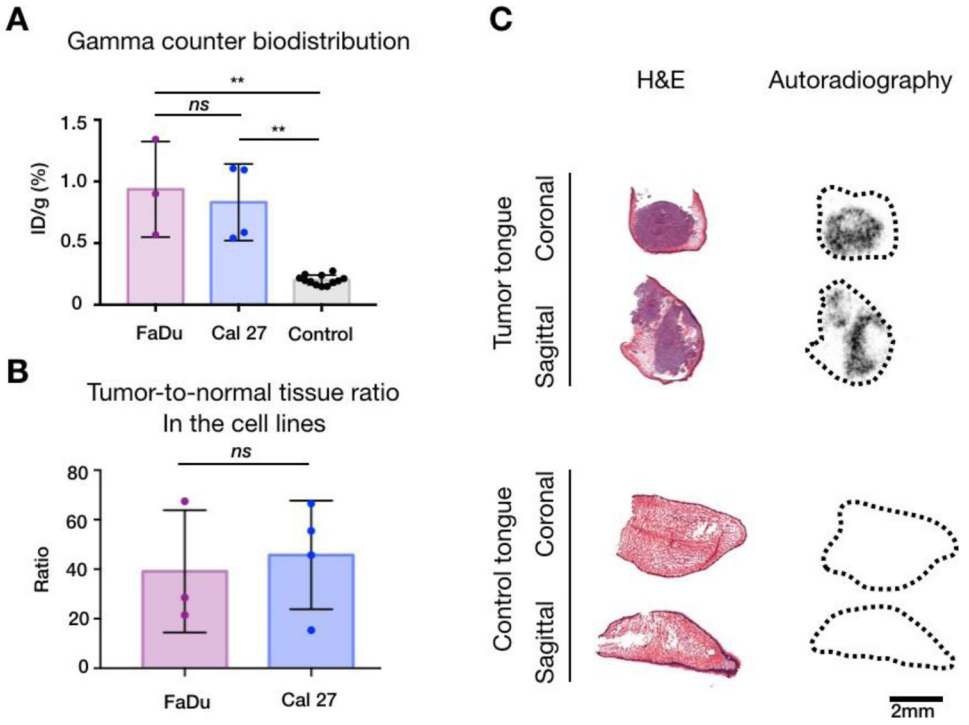

Fig 3.

Radiation emitted by tumor-bearing and controls tongues. **(A)** Gamma counter quantification of the [^{18}F]PARPi tracer uptake in healthy and tumor-bearing mouse tongues. Mauve = FaDu, blue = Cal 27 and black = Control tongues. Data points represents mean tracer uptake per tongue ± SD. (** $p < 0.01$, ns: $p > 0.05$ - Mann Whitney test). **(B)** Autoradiography quantification of tumor-to-normal tissue ratios. When analyzing all cell lines, the ratio was 42.9 ± 21.4. When separating by cell lines, FaDu (mauve) yielded a tumor-to-normal tissue ratio of 39.1 ± 24.7 and Cal 27 (blue) 45.8 ± 2, with no statistical significance between them ($p > 0.05$ – Mann Whitney test). **(C)** Representative images correlating autoradiography and histology. Slides were exposed to the autoradiography plate for 12 hours and read the next day before being stained for H&E. Almost all radiation arouse from the xenografts within the tongues (top). Almost no radiation arouses from the control tongues (bottom).

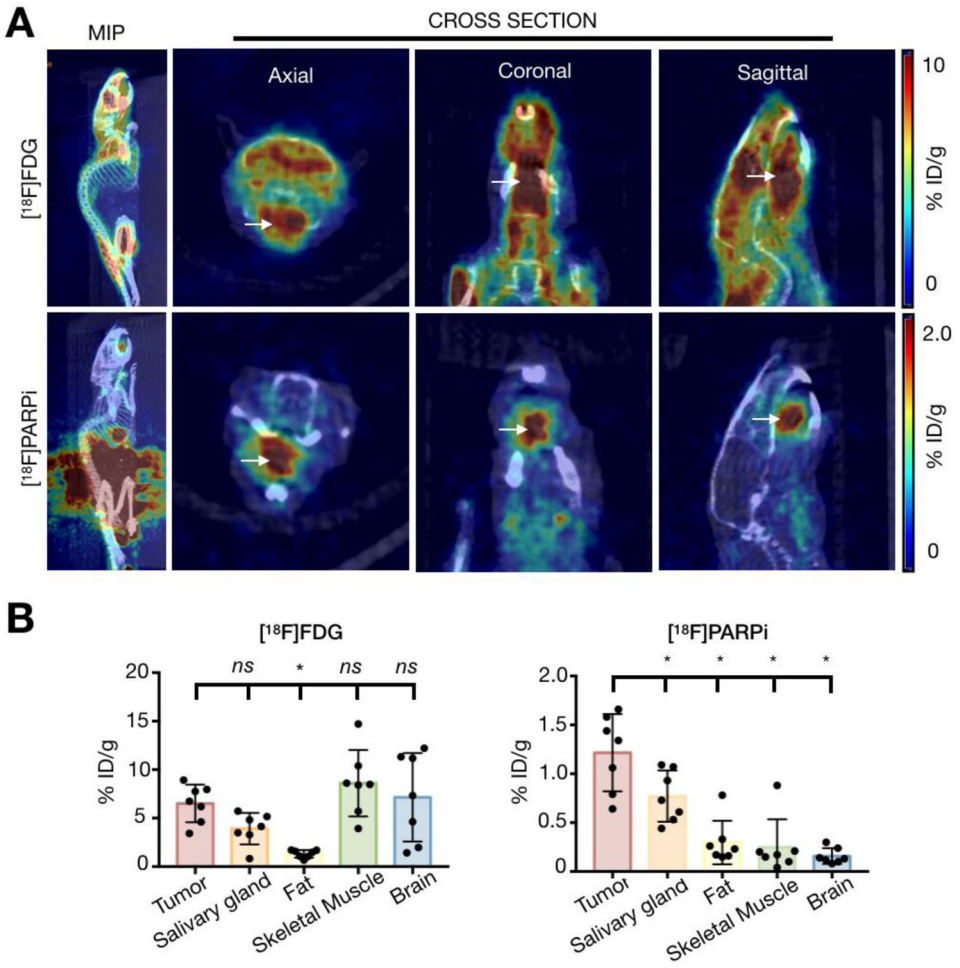

Fig 4.

PET imaging with [^{18}F]FDG and [^{18}F]PARPi. Animals were inoculated on the anterior 1/3 and ventral portion of the right-hand side of the tongue with 500,000 cancer cells in 20 μL of PBS (n = 3 FaDu, n = 4 Cal 27), and tumors were allowed to proliferate for 4 weeks. Mice were injected with an average of 7.7 ± 2.2 MBq (208.1 ± 59.4 μCi) of [^{18}F]FDG on Day 1 after tumor establishment and an average of 10.4 ± 3 MBq (282.2 ± 80.6 μCi) of [^{18}F]PARPi on Day 2, and imaged under isoflurane anesthesia for 15 minutes, 90 minutes after injection. Animals were imaged on an INVEON small-animal micro-PET/CT scanner under isoflurane-induced anesthesia. **(A)** Representative images of the PET/CT scans taken from the same mouse on consecutive days. The top row shows [^{18}F]FDG, imaged on Day 1, and the bottom row shows [^{18}F]PARPi, imaged on Day 2. Arrows point to the tumor. Images show clear, improved tumor delineation with [^{18}F]PARPi relative to [^{18}F]FDG. [^{18}F]FDG scans show high physiological uptake in the tongue, floor of mouth, and masticatory muscles. **(B)** Quantification of tracer uptake in different organs from PET/CT images of [^{18}F]FDG and [^{18}F]PARPi, respectively. Statistical analysis was performed using the Wilcoxon test in GraphPad Prism 7. Data points represent mean values, and error bars represent standard deviations. [^{18}F]FDG quantification showed that the uptake in tumor was not significantly different from the other organs, except for fat (*P < 0.05). [^{18}F]PARPi

quantification showed that the tracer had higher uptake in tumor than in salivary glands, fat, skeletal muscle and brain (*P < 0.05). [^{18}F]PARPi-PET allowed delineation of tumor from healthy tissue whereas [^{18}F]FDG failed to do so.

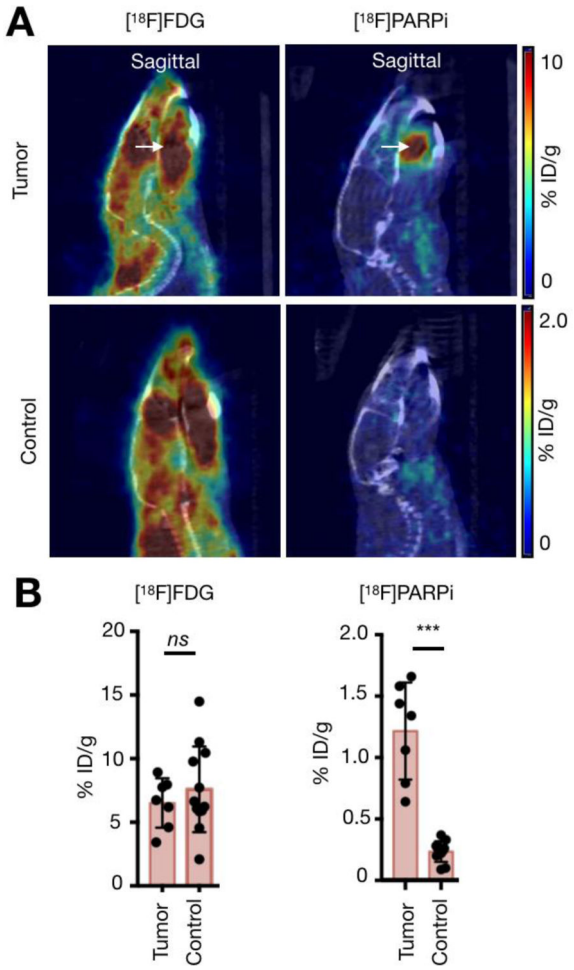

Fig 5.

PET imaging with [^{18}F]FDG and [^{18}F]PARPi. Tumor-bearing and control mice were injected with an average of 7.7 ± 2.2 MBq (208.1 ± 59.4 μCi) of [^{18}F]FDG on Day 1 and an average of 10.4 ± 3 MBq (282.2 ± 80.6 μCi) of [^{18}F]PARPi on Day 2, and imaged under isoflurane anesthesia for 15 minutes, 90 minutes after injection on an INVEON small-animal micro-PET/CT scanner under isoflurane-induced anesthesia. **(A)** Representative images of the PET/CT scans taken from a tumor-bearing (top row) and a control (bottom row) mouse with the different tracers on consecutive days. Arrows point to the tumor. Images show clear tumor delineation with [^{18}F]PARPi relative to control. Almost no uptake of the tracer was seen in controls. [^{18}F]FDG scans showed high physiological uptake in the tongue, floor of mouth, and masticatory muscles in both tumor-bearing and control mice. **(B)** Quantification of the two tracers in the xenografted and control tongues with [^{18}F]FDG (first column) and [^{18}F]PARPi (second). Statistical analysis was performed using the Mann Whitney test in GraphPad Prism 7. Data points represent mean values, and error bars represent standard deviations. [^{18}F]FDG quantification showed that the uptake in tumor-bearing tongues was not significantly different from the uptake in controls ($p > 0.05$). [^{18}F]PARPi quantification showed that the tracer had higher uptake in xenografted tongues when compared to controls

(***$p < 0.001$). [^{18}F]PARPi-PET allowed delineation of tumor whereas [^{18}F]FDG failed to do so.